ACS Sustainable Chemistry & Engineering

pubs.acs.org/journal/ascecg

Research Article

Finding Sustainable Deep Eutectic Solvents for an Efficient Separation of CO_2 and NH_3 in Melamine Production with Soft-SAFT

Luan Vittor Tavares Duarte de Alencar, Sabrina Belén Rodríguez-Reartes, Frederico Wanderley Tavares, and Fèlix Llovell*

Cite This: *ACS Sustainable Chem. Eng.* 2025, 13, 15097−15106

Read Online

ACCESS | Metrics & More | Article Recommendations | Supporting Information

ABSTRACT: Industrial processes frequently release tail gases containing harmful components, such as carbon dioxide (CO_2) and ammonia (NH_3), with significant environmental implications. Effective separation and recovery of these gases are critical for reducing pollution and enhancing resource efficiency. This paper investigates the use of deep eutectic solvents (DESs) to capture and separate CO_2 and NH_3 from melamine production tail gases, offering an alternative to traditional methods such as coproduction systems and water scrubbing. Choline chloride ([Ch]Cl)-based solvents with ethylene glycol (EG), urea (UR), and glycerol (GL) are assessed for selective gas absorption using the soft-SAFT Equation of State (EoS). This approach has been used to model the solubility of CO_2 and NH_3 in these DESs and evaluate key properties, including absorption isotherms, enthalpy, entropy of dissolution, effective Henry's constants, and ideal selectivity. Results reveal that the presence of EG enhances the NH_3 absorption capacity, while UR shows higher CO_2 absorption. From this information, the competitive selectivity in a standard melamine tail gas mixture (60% NH_3 and 40% CO_2 in mole fraction) and DESs has been predicted. Among them, [Ch]Cl:EG shows the best selectivity, and the 1:7 proportion provides the optimal value for NH_3/CO_2 separation. This work highlights the potential of DESs for efficient gas separation, emphasizing the utility of molecular modeling as a precursor to experimental validation in the design of sustainable separation processes.

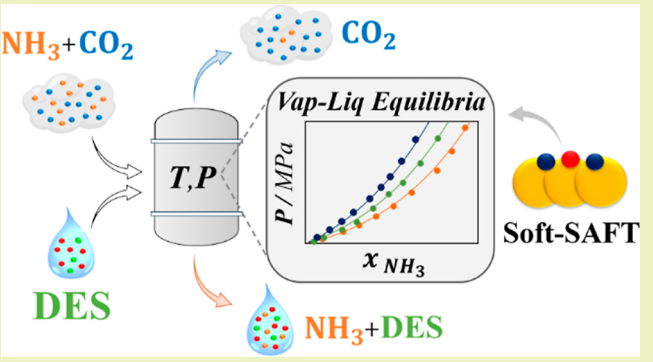

KEYWORDS: *deep eutectic solvents, solubility, soft-SAFT, carbon dioxide (CO_2), ammonia (NH_3), gas separation*

1. INTRODUCTION

Melamine ($C_3H_6N_6$) is a vital industrial raw material extensively utilized in manufacturing thermal insulation compounds, adhesives, and fibers.[1] Typically, the production of one ton of melamine through the decomposition and condensation of urea results in approximately 2.2 tons of tail gas, characterized by high concentrations of both NH_3 and CO_2.[2] Annually, the global production of melamine exceeds 1.59 million tons, leading to substantial exhaust greenhouse gas emissions.[3] This not only contributes to global warming, but also wastes valuable resources, as NH_3 is an important chemical building block used as a versatile agent in preparing many fine chemicals.[4,5] Therefore, an efficient separation and recovery of these gases can mitigate environmental impacts, enhance resource efficiency, and contribute to sustainable industrial practices.

According to literature reports, two primary methods have been developed for the simultaneous separation of NH_3 and CO_2 from gas mixtures. The first method involves coproducing urea or ammonium bicarbonate.[6,7] However, maintaining material balance in the coproduction system is challenging, and the excess of ammonia cannot be effectively utilized.[3] The second method is water scrubbing, which is effective in separating NH_3 and CO_2, but involves high utility consumption, making it an energy-intensive and costly process.[8]

A practical alternative method for NH_3 recovery from tail gas streams in melamine production involves absorption into ionic liquids (ILs). In particular, imidazolium-based ILs have proven to be cost-efficient compared to traditional water scrubbing techniques.[8,9] Additionally, the viability of IL-based NH_3 recovery from melamine tail gas has been demonstrated through the construction of the first industrial test pilot plant worldwide, developed by the Institute of Process Engineering, Chinese Academy of Sciences.[2] This plant, with a 50 N m^3 h^{-1} capacity and 3500 h of operation,[8] uses a specially designed IL with multiple hydrogen bonding sites, selected from a series of

Received: June 21, 2025
Revised: August 1, 2025
Accepted: August 4, 2025
Published: September 4, 2025

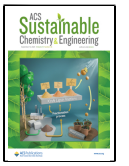

hydroxyl, protic, and metal ILs, to optimize NH_3 selectivity, stability, and energy efficiency.

The successful application of ILs comes at a certain cost associated with the synthesis of the solvent and some environmental concerns. Deep Eutectic Solvents (DESs) offer a promising alternative for gas capture, with lower toxicity, corrosivity and cost.[10] A DES consists of a liquid mixture of two or more hydrogen bonding components, which exhibits a significant depression in its melting point compared to that of their constituents, due to the hydrogen bond interactions between the hydrogen bond donor (HBD) and the hydrogen bond acceptor (HBA) compounds conforming the system.[11,12] The unique properties of DESs have garnered significant attention in various fields, including separation processes and gas capture technologies.[13−19] These solvents enable selective extraction, offering a sustainable alternative to traditional solvents. Extensive literature supports the adoption of DESs for capturing CO_2[15,20−23] and NH_3.[24−27]

The capability of DESs for gas absorption will depend on the selection of the two compounds forming the eutectic mixture and the proportion between them. Given the many possibilities, reliable predictive models are needed to quickly screen key thermodynamic properties, such as gas solubility and selectivity between gases. Many different thermodynamic models are available, ranging from quantum and molecular simulations, until cubic and molecular-based equations of state (EoS). Among them, SAFT-type equations of state[28,29] are attractive for modeling DESs due to their ability to explicitly account for hydrogen bonding. For instance, the well-known PC-SAFT version[30] has been successfully applied to predict CO_2 solubility in various DESs.[31,32] Also, the soft-SAFT EoS,[33] has also been used to describe the absorption of gases in DESs, showing accurate predictions for the solubilities of CO_2[34−36] and fluorinated gases,[37,38] among other modeled compounds.

This work aims to analyze the solubility of CO_2 and NH_3 in three different choline chloride ([Ch]Cl)-based DESs formed with ethylene glycol (EG), urea (UR), and glycerol (GL). The ideal selectivity of NH_3 over CO_2 in these DESs is examined, along with the prediction of absorption isotherms, the enthalpy and entropy of dissolution, and the Henry's constants. Furthermore, the study predicts the competitive selectivity of NH_3 over CO_2 in multicomponent mixtures based on melamine tail gas and DESs. From these analyzes, a rational discussion is made to identify the most suitable DES for efficient NH_3 recovery from the tail gas, supporting the initial phase of design of an industrial gas separation unit.

2. METHODOLOGY

2.1. The Soft-SAFT Equation of State. The general expression for the soft-SAFT EoS[33] computes the residual Helmholtz energy (A^{res}) by summing different microscopic contributions to a given molecule, as

$$A^{res} = A^{ref} + A^{chain} + A^{assoc} + A^{polar} \quad (1)$$

In eq 1, the reference term (A^{ref}) accounts for segment−segment interactions via the Lennard-Jones potential, calculated using the Johnson et al. EoS[39] within soft-SAFT. The chain term (A^{chain}) describes the connectivity of segments into chains, while the association term (A^{assoc}) captures strong, short-range directional interactions from hydrogen bonding. Both terms stem from Wertheim's first-order thermodynamic perturbation theory[40−43] and are formally identical across all SAFT variants. An additional polar term (A^{polar}) is included to capture long−range interactions such as CO_2 quadrupolar forces, based on the theory of Gubbins and Twu[44] (initially developed for spherical molecules) and later extended to chain fluids following the ideas of Jog et al.[45] Further details about the model and the inclusion of the polar term can be found in the original contributions.[46,47]

Thermodynamic modeling with soft-SAFT requires molecular parameters describing structural and energetic characteristics. For nonassociating compounds, three parameters are used: chain length (m), segment diameter (σ), and dispersive energy (ε). For associating systems, two extra parameters, the association volume (κ^{HB}) and energy (ε^{HB}), are included. These are typically fitted to experimental data. For polar compounds, the polar moment (μ/Q) and the polar segment fraction (x_p) are specified. The polar moment is often taken from experimental sources while x_p is set a priori based on physical arguments.[33,46]

The extension to mixtures is straightforward for the chain, association, and polar terms, as they are specifically written for a multicomponent case. For the reference term, the van der Waals one-fluid theory is applied, using unlike size and energy parameters of the Lennard-Jones fluid obtained via the generalized Lorentz−Berthelot rules (eqs 2 and 3)

$$\sigma_{ij} = \eta_{ij}\frac{(\sigma_{ii} + \sigma_{jj})}{2} \quad (2)$$

$$\varepsilon_{ij} = \xi_{ij}\sqrt{\varepsilon_{ii}\varepsilon_{jj}} \quad (3)$$

where η_{ij} and ξ_{ij} are the adjustable size and energy binary interaction parameters between species i and j. These parameters account for asymmetry and nonidealities between the different natures of the mixture compounds. They can be fitted to binary experimental data if predictions from the pure components ($\eta_{ij} = \xi_{ij} = 1$) are unsatisfactory.

For mixtures of compounds with hydrogen-bonding interactions, cross-association between different molecules or functional groups within the same type of molecules are calculated using combining rules, in a similar manner as done in eqs 2 and 3. When energies and volumes between a site type A in component i and a site type B in component j are required, the following equations are applied

$$\varepsilon^{HB}_{AB,ij} = \alpha^{HB}_{ij}\sqrt{\varepsilon^{HB}_{AB,ii}\varepsilon^{HB}_{AB,jj}} \quad (4)$$

$$k^{HB}_{AB,ij} = \left(\frac{\sqrt[3]{k^{HB}_{AB,ii}} + \sqrt[3]{k^{HB}_{AB,jj}}}{2}\right)^3 \quad (5)$$

where α^{HB}_{ij} acts as a correction factor for the cross-association energy and can be fitted to experimental binary data if the default assumption ($\alpha^{HB}_{ij} = 1$) does not provide a suitable description of the system.

2.2. Molecular Models. To accurately describe the thermodynamic behavior of the studied systems, each compound was represented using a molecular model tailored to its structural and interaction characteristics. A summary of these representations, including molecular structures and corresponding soft-SAFT models used in this work are summarized in Figure S1 of the Supporting Information. Following a previous contribution,[48] [Ch]Cl:UR (1:2), [Ch]Cl:EG (1:2), and [Ch]Cl:GL (1:2) were modeled using the individual-component approach, where each entity is

https://doi.org/10.1021/acssuschemeng.5c06167
ACS Sustainable Chem. Eng. 2025, 13, 15097−15106

Table 1. Soft-SAFT Molecular Parameters Optimized for the Species That Form the Deep Eutectic Solvents and the Gases Studied in This Work

compound	M_w (g/mol)	m	σ (Å)	ε/k_B (K)	ε^{HB}/k_B (K)	k^{HB} (Å^3)	No. of sites	Reference
[Ch]Cl	139.63	5.096	3.401	428.40	3384	2100	1 + 1	48
UR	60.06	2.458	3.090	420.70	3384	2100	1 + 1	48
EG	62.07	1.751	3.668	326.05	4384	4195	1 + 1	49
GL[a]	92.09	2.397	3.638	392.95	4945	2250	1 + 1	50
CO_2	44.01	1.571	3.184	160.2				51
NH_3	17.04	1.873	2.679	236.5	1136	1498	3 + 1	this work

[a]Additional molecular parameters for the polar contribution: $Q = 4.40 \times 10^{-40}$ C·m^{-2}, $x_p = 1/3$.

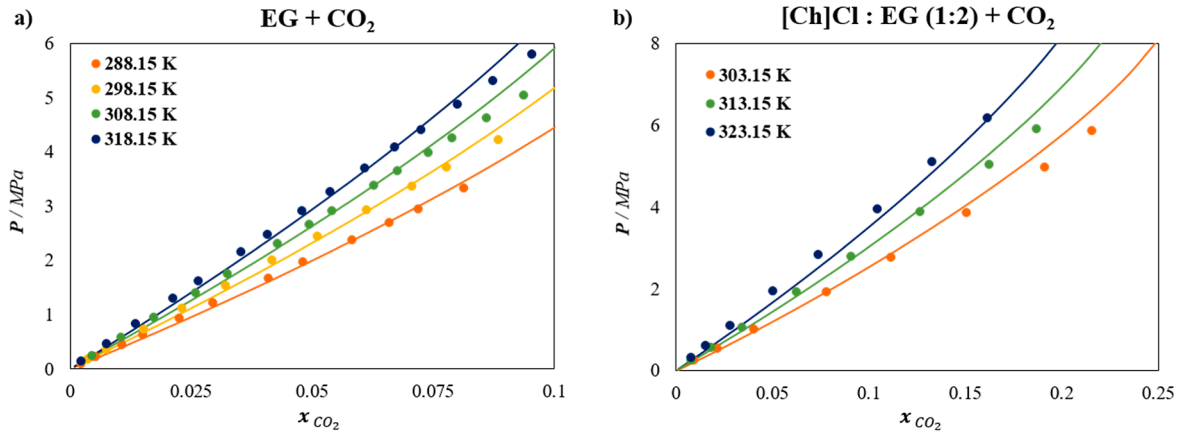

Figure 1. Solubility of CO_2 at different temperatures in (a) EG and (b) [Ch]Cl:EG (1:2) DES. Symbols represent experimental data[53,54] and lines are soft-SAFT calculations.

characterized by a specific set of parameters. All compounds were modeled with two different association sites (A and B), to simulate the positively and negatively charged regions in the molecule, respectively. A-B interactions are allowed to represent the HBA−HBD associations. In prior works, the parameters of EG[49] and GL[50] had already been adjusted to vapor−liquid equilibrium (VLE) data (saturated liquid density and vapor pressure), while the parameters for [Ch]Cl and UR were later obtained by fitting to DES single-phase density data,[48] as these fluids exhibit negligible vapor pressures. These parameters were used in this current work.

Additionally, CO_2 is modeled as a Lennard-Jones (LJ) nonassociating chain, but explicitly incorporates quadrupolar interactions through the polar term. For CO_2, x_p was fixed at 1/3, representing that only one-third of the molecule is affected by the quadrupolar interactions. Departing from the experimental value, the effective quadrupole moment for CO_2 ($Q = 4.40 \times 10^{-40}$ C·m^{-2}) was refined from fitting. The final set of molecular parameters for CO_2 was taken from Dias et al.[51] Finally, a four-site model is proposed for NH_3, following the ideas of Llovell et al.,[52] with three H-type sites representing the hydrogen atoms and one e-type site representing the lone pair of electrons on nitrogen. Only e−H associating interactions are allowed. Although a set of soft-SAFT parameters is available in the literature for NH_3,[52] some deviations in the description of the saturated liquid density were found at the range of temperatures of interest for this work (280−360 K), with an % AAD of 7.03%. This temperature range is crucial for the current study on the absorption of NH_3 from tail gas in melamine production with DESs. Consequently, a new parametrization has been carried out for NH_3 using saturated liquid density and vapor pressure data, achieving a better fit to the VLE of ammonia in the range of interest, with an % AAD of 1.02% in the 275−375 K range. The description of the VLE equilibrium properties of ammonia with both parameter sets can be found in Figure S2 of the Supporting Information (see also Table S1 for the corresponding parameter values). A summary of the parameters for all compounds is provided in Table 1.

3. RESULTS

3.1. Solubility of CO_2 in [Ch]Cl Based-DESs. A quantitative and reliable description of the process requires accounting for the binary interactions between all components in the system. As DESs are intrinsically binary mixtures (although it is possible to have also ternary or multicomponent DESs), it is necessary to consider the interactions of each gas with both constituents. Consequently, and before proceeding to evaluate the solubility of CO_2 in the selected DESs, the binary system CO_2-EG, for which experimental data were available,[53] has been first examined.

Results concerning the soft-SAFT description of the VLE for the mixture between EG and CO_2 at different temperatures are depicted in Figure 1a and compared to experimental data.[53] As can be seen, an excellent agreement is achieved (%AAD of 3.06%) by setting a constant binary parameter ξ_{EG-CO_2} = 0.886. This parameter was fitted to data at 298.15 K and used to predict the other three isotherms at 288.15, 308.15, and 318.15 K, ensuring that a temperature-independent parameter can accurately reproduce the system at different conditions.

The next step concerns the description of the CO_2 solubility in the selected DES [Ch]Cl:EG 1:2, considering it as a ternary mixture. HBA−HBD interactions are always described without involving any binary parameter ($\xi_{HBA-HBD}$ = 1.00), regardless of the type of HBD employed. Moreover, the ξ_{EG-CO_2} value

https://doi.org/10.1021/acssuschemeng.5c06167
ACS Sustainable Chem. Eng. 2025, 13, 15097−15106

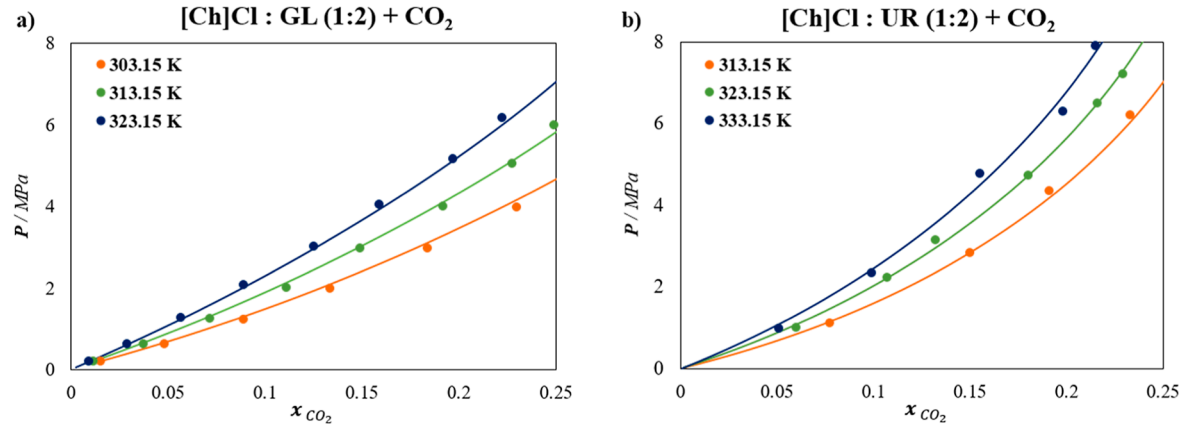

Figure 2. Solubility of CO_2 at different temperatures in (a) [Ch]Cl:GL (1:2) DES, and (b) [Ch]Cl:UR (1:2) DES. Symbols represent experimental data,[55,56] and lines are soft-SAFT calculations.

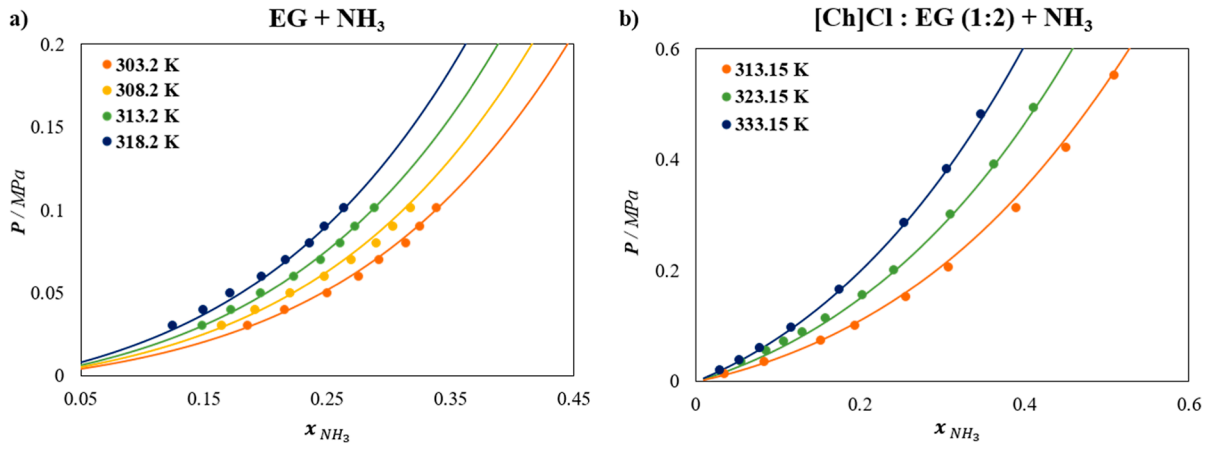

Figure 3. Solubility of NH_3 at different temperatures in (a) EG, and (b) [Ch]Cl:EG (1:2) DES. Symbols represent experimental data,[57,59] and lines are soft-SAFT calculations.

previously fitted, accounting for the HBD−CO_2 interaction, has been transferred to address the EG−CO_2 interaction in the ternary mixture DES + CO_2, while the ξ parameter describing the interaction between [Ch]Cl (HBA) and CO_2, has been fitted to the ternary data. In particular, the intermediate temperature isotherm was used to obtain an optimum $\xi_{[Ch]Cl-CO_2}$ value of 1.10, while the other two isotherms were predicted using this value. The results are plotted in Figure 1b, evidencing excellent agreement with the CO_2 solubility data across all isotherms, with an % AAD of 6.02%.

The subsequent step involves describing the CO_2 solubility in other DESs with different HBDs (GL and UR). The $\xi_{[Ch]Cl-CO_2}$ previously fitted (see Figure 1b) has been transferred to the other two [Ch]Cl-based DESs, provided that this binary interaction is independent of the HBD. Additionally, the ξ_{HBD-CO_2} values, corresponding to UR and GL with CO_2, have been fitted to the corresponding ternary data. In both cases, the intermediate temperature isotherm was used to obtain optimal ξ values, while the other two isotherms were predicted. A summary of the necessary ξ values to quantitatively describe the CO_2 solubility in DESs is provided in Table S2 of the Supporting Information.

No further adjustments are necessary for the Lorentz combining rule (η = 1), which is consistently applied across all binary combinations, except for [Ch]Cl:UR (1:2), where a constant η value of 0.9 between UR and CO_2 is necessary. This variation may potentially be attributed to the findings from Crespo et al.,[50] which suggested that different types of hydrogen bonds may form in the [Ch]Cl:UR (1:2) mixture beyond what simplified models can accurately capture. In our approach, these interactions have been simplified to two association sites each for [Ch]Cl and UR to facilitate the transferability of soft-SAFT parameters, possibly underestimating specific interactions. Figure 2 displays the results for the [Ch]Cl-based DESs with UR, and GL in a (1:2) ratio. Overall, this approach yields an excellent description of the CO_2 solubility across various isotherms for the DESs, with an % AAD of 3.24% and 5.17% for [Ch]Cl:GL (1:2) and [Ch]Cl:UR (1:2), respectively.

3.2. Solubility of NH_3 in [Ch]Cl Based-DESs. In a similar approach to that used for CO_2 solubility, the solubility of NH_3 in DESs must first be characterized by accurately describing the binary interactions. First, EG-NH_3 has been evaluated with soft-SAFT and fitted to available experimental data.[57] While CO_2 was modeled as a nonassociating (but polar) compound, the associating nature of ammonia, represented by 4 sites in soft-SAFT, allows the optimization of the cross-association interactions between NH_3 and the DESs components, given their substantial influence on the thermophysical property predictions in such mixtures.[52] Notice that these interactions correspond to the e−A (negative−positive) and H−B (positive−negative) interactions between NH_3 and EG, while

https://doi.org/10.1021/acssuschemeng.5c06167
ACS Sustainable Chem. Eng. 2025, 13, 15097−15106

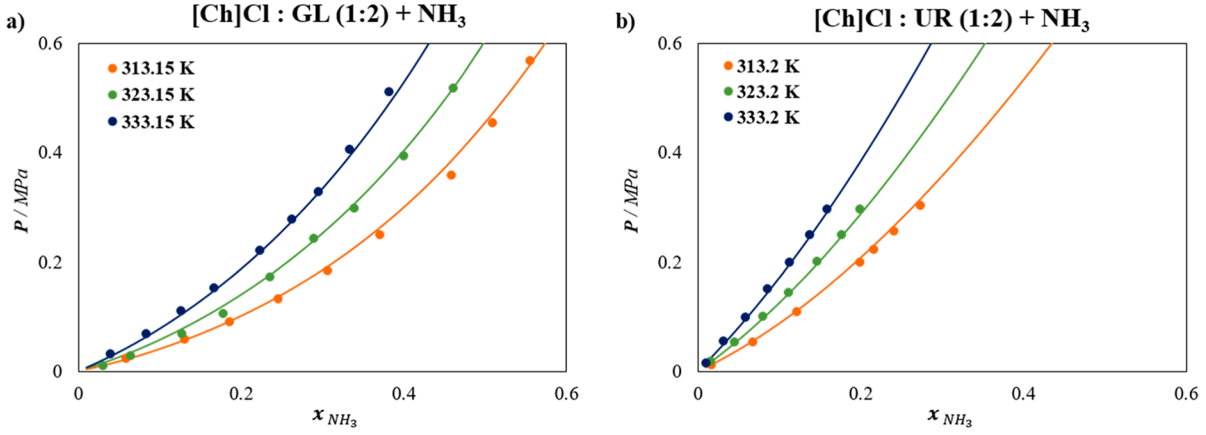

Figure 4. Solubility of NH_3 at different temperatures in (a) [Ch]Cl:GL (1:2) DES, and (b) [Ch]Cl:UR (1:2) DES. Symbols represent experimental data,[24,59] and lines are soft-SAFT calculations.

e−B and H−A were set to zero (same sign). To optimize these interactions, suitable values for cross-association parameters were determined within a logical range based on the physical interpretation of chemical reactions. Specifically, the correction factor for the cross-association energy, $\alpha^{HB}_{EG-NH_3} = 1.386$, was found from fitting to experimental VLE data for the EG + NH_3 system (Figure 3a), as the default value ($\alpha^{HB}_{EG-NH_3} = 1$) did not satisfactorily describe the experimental behavior. This adjustment increased the cross-association energy between EG and NH_3 from 2231.64 to 3093 K, reinforcing the presence of strong hydrogen bonding interactions, as also reported through Ab Initio Molecular Dynamics evidences by Malik and Kashyap.[58]

Additionally, the size binary interaction parameter η_{EG-NH_3}= 0.9 was also fitted to better capture the behavior of the system in the whole range of compositions, while the dispersive energy binary parameter ξ_{EG-NH_3} was set to 1, as the complex interactions are assumed to be effectively captured by the cross-association value. These fittings were performed at an intermediate temperature of 313.2 K and then applied in a transferable manner to predict the solubility at other temperatures. The results of the soft-SAFT description of the VLE for the EG−NH_3 mixture at various temperatures are presented in Figure 3a. Good agreement between experimental data[57] and the soft-SAFT model is found, with an % AAD of 2.01%.

Once the EG−NH_3 mixture has been accurately described, the ternary system [Ch]Cl:EG + NH_3 is evaluated and taken as the benchmark system to estimate all necessary binary parameters. As far as the EG−NH_3 interactions are transferred from the previous study (Figure 3a), and no binary parameters are required for the HBA/HBD, the remaining interaction parameters between the salt ([Ch]Cl) and NH_3 were fitted to adjust the ternary mixture of [Ch]Cl:EG (1:2) + NH_3, obtaining $\xi_{[Ch]Cl-NH_3} = 0.80$ and $\eta_{[Ch]Cl-NH_3} = 1.030$ across all isotherms. Figure 3b shows the results for [Ch]Cl:EG (1:2) + NH_3, demonstrating an excellent description of the NH_3 solubility across various isotherms for this DES, with an % AAD of 4.45%.

The ξ and η parameters between NH_3 and [Ch]Cl were subsequently transferred to mixtures of NH_3 with the other two [Ch]Cl-based DESs studied, GL and UR. No further adjustments for ξ_{HBD-NH_3} were necessary, while the remaining η_{HBD-NH_3} values were optimized to a constant value of 0.97 for GL and UR using the intermediate temperature isotherm, with predictions extended to the other two isotherms. Finally, cross-association energy parameters were also determined between NH_3 and the other HBDs, requiring the use of correction factors $\alpha^{HB}_{GL-NH_3} = 1.442$ and $\alpha^{HB}_{UR-NH_3} = 1.359$, respectively. These adjustments increased the cross-association energy between GL and NH_3 from 2370.13 to 3418 K, and between UR and NH_3 from 1960.67 to 2665 K, indicating strong hydrogen bonding interactions. These parameters were also fitted using an intermediate isotherm at 323.15 K. A summary of all the necessary η_{ij} and the correction factor for the cross-association energy values for quantitatively describing the NH_3 solubility in DESs is provided in Table S3 of the Supporting Information.

The description of the solubility of NH_3 in [Ch]Cl-based systems with GL and UR in a (1:2) ratio is illustrated in Figure 4, with % AAD values of 6.94% and 3.01%, respectively. It is important to remark that no degeneracy of the model is observed when predicting the behavior of other isotherms not used in the fitting.

3.3. Enthalpy and Entropy of Dissolution. Beyond solubility, the absorption enthalpy and entropy also play key roles in CO_2 and NH_3 uptake by DESs. These properties offer valuable insights into the energetic and structural changes occurring upon gas dissolution in DESs,[60] and can be predicted using soft-SAFT and standard thermodynamic expressions

$$\Delta H_{dis,i} = -RT^2\left(\frac{d\ln P_i}{dT}\right)_{x_i} \quad (6)$$

$$\Delta S_{dis,i} = -RT\left(\frac{d\ln P_i}{dT}\right)_{x_i} \quad (7)$$

where $\Delta H_{dis,i}$ and $\Delta S_{dis,i}$ are the molar enthalpy and entropy of dissolution, R is the universal gas constant (8.3145 J·mol^{-1}·K^{-1}), P_i is the partial pressure of the dissolved of gas i, T is the overall system temperature, and x_i is the mole fraction of the dissolved gas i in the DESs (fixed at 0.01 to represent dilute conditions). The corresponding values for each gas in the respective DES are summarized in Table S4 of the Supporting Information.

The results show that ΔH_{dis} values are consistently more negative for NH_3 than for CO_2 across all DESs, indicating that

https://doi.org/10.1021/acssuschemeng.5c06167
ACS Sustainable Chem. Eng. 2025, 13, 15097−15106

NH_3 dissolution is more exothermic. Similarly, ΔS_{dis} values are negative for both gases, mainly attributed to gas condensing, being also more negative for NH_3. The reduction in entropy due to this phase transition is not compensated by the entropy generated from the disruption of CO_2 or NH_3 into the ordered structure of the DESs.

3.4. Impact of the HBD and HBA/HBD Proportion in the Ideal Selectivity. The capability of an absorbent to selectively capture a specific gas from a mixture is essential for optimizing gas recycling and separation processes. In this regard, evaluating the selectivity between CO_2 and NH_3 appears as a key performance indicator to check the potential of DESs for this separation. Consequently, the ideal selectivity of CO_2 and NH_3 in the three DESs was calculated to prescreen their efficiency in separating these gases. The ideal selectivity at infinite dilution is obtained as the ratio of the effective Henry's law constants for the two pure gases. It indicates the relative solubility of each gas in the DES at a given isotherm,[61] as follows

$$\beta_{i/j}^{T} = \frac{k_{H,eff}^{j\,T}}{k_{H,eff}^{i\,T}} = \frac{\lim_{x_j \to 0}\left(\frac{P}{x_j}\right)^{T}}{\lim_{x_i \to 0}\left(\frac{P}{x_i}\right)^{T}} \quad (8)$$

where $k_{H,eff}^{i}$ represents the effective Henry's law constant[62] for gas i at temperature T, x_i denotes the molar fraction of compound i in the liquid, and $\beta_{i/j}$ represents the ideal selectivity at infinite dilution of the compound j concerning the compound i.

In this work, soft-SAFT is used to predict pressure data as solubility approaches zero for each isotherm and compound, allowing to evaluate the effective Henry's law constants and the ideal selectivity. The results are graphically shown in Figure 5a at 313.15 K, while the list of values at all temperatures investigated are included in Tables S5 and S6 of the Supporting Information. The effective Henry's constants are directly linked to the solubility measurements shown in Figures 1−4. In general, all DESs exhibit larger values of effective Henry's constants (i.e., lower affinity) for CO_2 than for NH_3. The values of CO_2 absorption are in agreement with those reported in the literature for ammonium salt-based DESs.[35,36] As illustrated in Figure 5a (blue bars graph, left axis), [Ch]Cl:UR (1:2) shows the lowest $k_{H,eff}$ for CO_2, indicating a higher absorption capacity, followed by [Ch]Cl:GL (1:2) and [Ch]Cl:EG (1:2). Contrarily, [Ch]Cl:UR shows the highest $k_{H,eff}$ for NH_3 (orange bars graph, left axis), indicating a lower absorption capacity, while the other DESs exhibit lower similar values of $k_{H,eff}$ for NH_3.

Regarding the ideal selectivity of NH_3/CO_2 shown in Figure 5a (symbols and lines, right axis), the highest β_{NH_3/CO_2} value (77.108) among the investigated DESs for the binary mixtures is achieved with [Ch]Cl:EG (1:2), indicating the best selectivity and preference for NH_3 in this mixture. Based on these preliminary results, [Ch]Cl:EG is preselected as the most suitable DES for NH_3−CO_2 separation.

While the [Ch]Cl:EG HBA:HBD combination seems to offer the most promising performance, it is interesting to check the influence of the molar ratio of this DES on the selectivity of NH_3 over CO_2. Of course, this range will be limited by the eutectic point, so it is known that a minimum ratio of

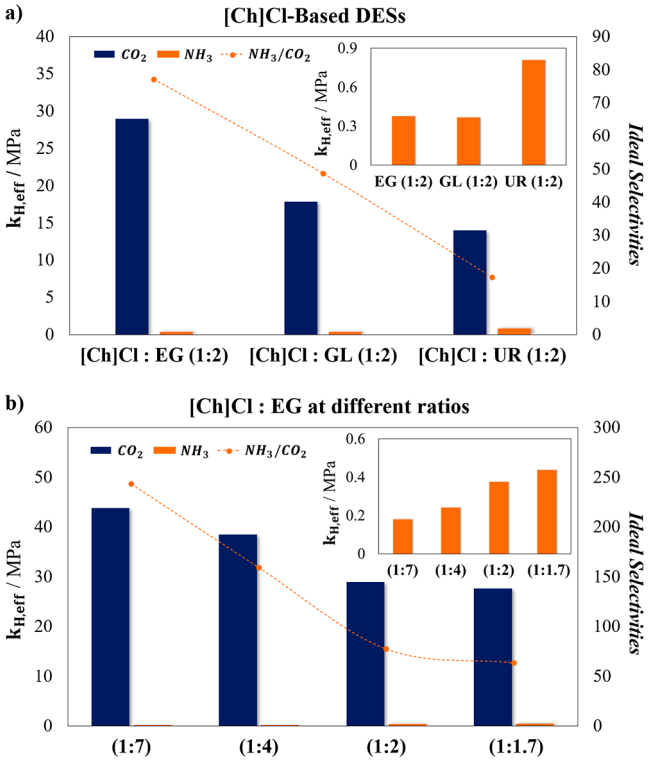

Figure 5. Calculated effective Henry's constants ($k_{H,eff}$) for CO_2 and NH_3 (bars graph, left axis) and ideal selectivity (β_{NH_3/CO_2}, symbols and lines, right axis) at 313.15 K: (a) for [Ch]Cl:EG (1:2), [Ch]Cl:GL (1:2), and [Ch]Cl:UR (1:2); and (b) for [Ch]Cl:EG at different molar ratios.

approximately 1:1.7 is needed to avoid the solidification of the solvent in the range of temperatures studied.[63,64]

Using soft-SAFT, the solubility of both gases in [Ch]Cl:EG is predicted at different HBA:HBD proportions and compared to the [Ch]Cl:EG (1:2) system. The analysis includes higher ratios (1:4) and (1:7) of EG, for which experimental data were available.[65] Even in the absence of data, the low ratio (1:1.7) was also predicted to assess the effect of reduced EG content. As shown in Figure S3 of the Supporting Information, the soft-SAFT model provides good agreement with the available NH_3 experimental data, yielding an overall % AAD of 8.07%. All calculations were made in a fully predictive manner using the molecular parameters optimized for the [Ch]Cl:EG (1:2) system (Figure 3), without the need for any additional parameter adjustments, demonstrating the robustness and transferability of the model to different DES compositions. In the case of CO_2, no experimental solubility data were available for [Ch]Cl/:EG at different ratios, and soft-SAFT predictions at various molar ratios are presented in Figure S4 of the Supporting Information.

The results of these absorption-isotherms predictions $k_{H,eff}^{i}$ of CO_2 and NH_3, as well as β_{NH_3/CO_2}, were estimated for the four DESs. Figure 5b illustrates both, $k_{H,eff}^{i}$ and β_{NH_3/CO_2}, for [Ch]Cl:EG at different molar ratios, while the exact values are summarized in Table S7 of the Supporting Information.

The results reveal that increasing the molar ratio of [Ch]Cl:EG from 1:2 to 1:7 decreases the CO_2 absorption capacity, as evidenced by the increase in $k_{H,eff}^{i}$ from 28.985 to 43.77. Conversely, this change increases the NH_3 absorption capacity, indicated by the decrease in the corresponding $k_{H,eff}^{i}$

https://doi.org/10.1021/acssuschemeng.5c06167
ACS Sustainable Chem. Eng. 2025, 13, 15097−15106

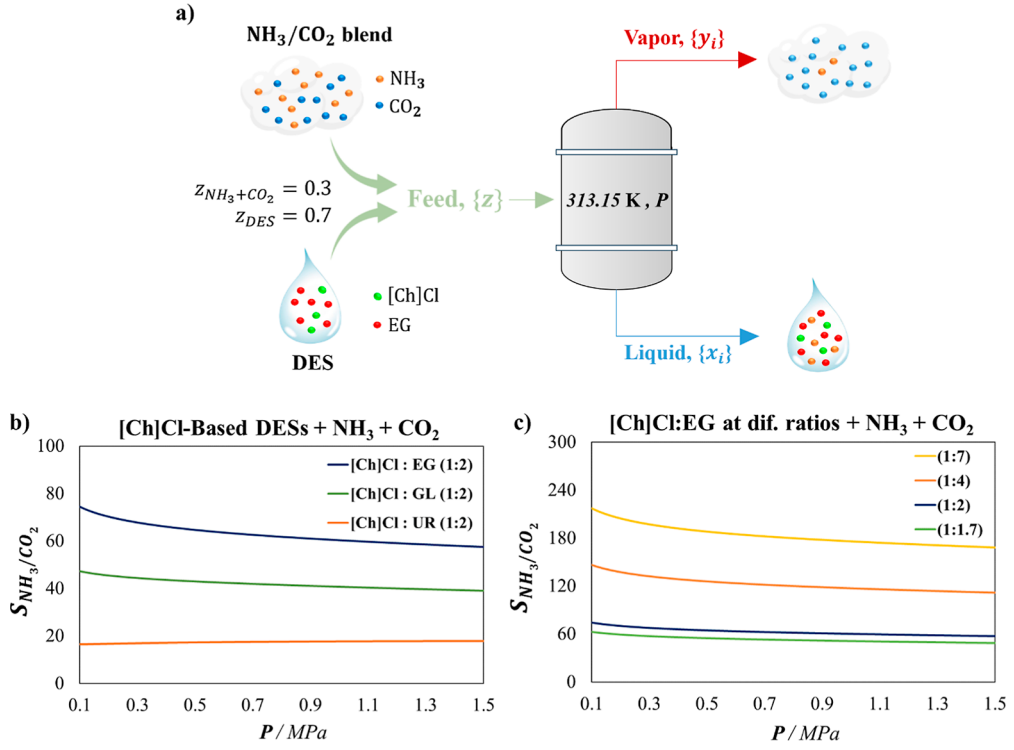

Figure 6. (a) Illustration of vapor−liquid flash calculations via soft-SAFT EoS depicting the separation performance of NH_3/CO_2 blends at 313.15 K and different pressures. NH_3 competitive selectivity over CO_2 in (b) [Ch]Cl-based DESs, and (c) [Ch]Cl:EG at different proportions. Global molar composition of the analyzed mixture of $z_{DES} = 0.7$ and $z_{CO_2+NH_3} = 0.3$ modeled using soft-SAFT EoS. The CO_2 + NH_3 blend contains 60% NH_3 and 40% CO_2 in mole fraction.

from 0.3759 to 0.18. When the molar ratio is decreased from 1:2 to 1:1.7, the opposite effect occurs. As a result, increasing the molar ratio from 1:2 to 1:7 leads to an approximate 215% increase in the ideal selectivity factor β_{NH_3/CO_2}, rising from 77.108 to 243.167. These findings suggest that tuning the HBA/HBD molar ratio is a promising strategy for enhancing NH_3 over CO_2 selectivity in [Ch]Cl:EG-based DESs.

3.5. Separation Performance in an NH_3/CO_2 Tail Gas from Melamine Production. The ideal selectivity calculated from effective Henry's coefficients is an approximation based on the infinite dilution behavior of pure compounds (CO_2 and NH_3 in this study). This method does not account for the competition between gases, providing only a preliminary indication of each DES's separation capacity. To accurately assess gas separation efficiency, competitive selectivity is evaluated here to simulate the recovery of NH_3 from melamine production tail gas. According to Duan et al.,[8] a melamine tail gas produced in China contains 7.6% N_2, 0.4% H_2O, 55% NH_3, and 37% CO_2 in mole fraction. In our study, this residual mixture has been simplified to a binary system containing 60% NH_3 and 40% CO_2 in mole fraction. Although a detailed analysis should include all the components present in the tail gas, our study focuses on the main constituents to enable an initial screening of the most suitable solvent. Indeed, it is expected that N_2 exhibit minimal solubility, acting mostly as an inert.[8] Concerning water, its content is very low, and its main effect in the system is expected to be a reduction of DES viscosity rather than having a significant influence on the relative solubilities of CO_2 and NH_3 in the solvent.

In this case, the values of competitive selectivity (S) calculated for these gas mixtures are obtained through eq 9

$$S_{i/j} = \frac{y_j/x_j}{y_i/x_i} \tag{9}$$

where x and y are the liquid and vapor molar fractions of each gas in the mixture, respectively. These compositions can be obtained from liquid−vapor flash calculations using soft-SAFT, which are computed by an iterative procedure that solves a modified multiphase Rachford−Rice equation mass balance.[66,67] The calculation assumes an initial global composition with a DES mole fraction of 0.7 ($z_{DES} = 0.7$) and 0.3 for the melamine tail gas blend ($z_{NH_3+CO_2} = 0.3$), the latter on a 60:40 mol % basis, as previously specified. A schematic diagram of the separation process is shown in Figure 6a. The separation performance of NH_3/CO_2 blends at 313.15 K and different pressures is shown in Figure 6b,c.

Overall, significant potential for achieving a high separation efficiency in the NH_3-CO_2 separation at the specified conditions is observed. The predicted competitive selectivity closely aligns with the ideal selectivity at infinite dilution, as seen when comparing Figure 5 with Figure 6. This correlation is especially evident at low pressures, where ideal conditions are predominant. However, while low pressures enhance separation performance, they come at the expense of reduced sorption capacity, as indicated in Figures 1−4, leading to a lower NH_3 recovery in quantitative terms. Conversely, high-pressure conditions do not yield favorable outcomes, as they decrease the NH_3-CO_2 separation efficiency for [Ch]Cl-based DESs. Therefore, based on this analysis, operating under moderate pressure conditions is recommended for efficient NH_3-CO_2 separation. Among the studied DESs, [Ch]Cl:EG

https://doi.org/10.1021/acssuschemeng.5c06167
ACS Sustainable Chem. Eng. 2025, 13, 15097−15106

(1:7) stands out as the best choice for NH_3 capture from melamine tail gas streams.

4. CONCLUSIONS

Aimed to find an optimal recovery process for the separation of CO_2 and NH_3 in melamine tail gas streams, a comprehensive study was conducted to model the solubility of these gases in three [Ch]Cl-based DESs, with EG, UR, and GL as HBDs, using the soft-SAFT EoS. The soft-SAFT calculations effectively described the isotherms of CO_2 and NH_3 in the three studied DESs over the temperature range of 303.15 to 333.15 K, showing excellent agreement with experimental data. Temperature-independent binary parameters for energy and size were adjusted between the DESs components and the studied gases to achieve this level of accuracy. Later, the soft-SAFT EoS was used to predict essential properties, including enthalpy and entropy of dissolution, effective Henry's constants, and ideal selectivity. Among the investigated DESs, [Ch]Cl:UR (1:2) demonstrated the highest CO_2 solubility, whereas [Ch]Cl:EG (1:2) exhibited the highest NH_3 absorption capacity at 313.15 K. The competitive selectivity of the NH_3/CO_2 mixture (60/40 mol % basis, simulating the tail gas composition from melamine production) in the DESs was evaluated at 313.15 K and in the 0.1−1.5 MPa pressure range. For the separation of NH_3 from CO_2 mixtures in melamine tail gas streams at 313.15 K, [Ch]Cl:EG (1:7) at moderate pressures emerged as the most effective DES among those studied solvents and conditions. Following this computational approach, experiments can be conducted with the selected entrainer to validate the results and refine the optimal conditions for the separation process, providing a more environmentally friendly solution to current industrial options.

■ ASSOCIATED CONTENT

Supporting Information

The Supporting Information is available free of charge at https://pubs.acs.org/doi/10.1021/acssuschemeng.5c06167.

Molecular structure representations; VLE curves and parameter comparison for NH_3; soft-SAFT solubility predictions and flash separation performance for CO_2 and NH_3 in [Ch]Cl-based DESs at different HBA/HBD ratios; calculated enthalpy and entropy of absorption; effective Henry's law constants and NH_3/CO_2 ideal selectivities values at various temperatures (PDF)

■ AUTHOR INFORMATION

Corresponding Author

Fèlix Llovell − *Department of Chemical Engineering, ETSEQ, Universitat Rovira i Virgili, 43007 Tarragona, Spain;* orcid.org/0000-0001-7109-6810; Email: felix.llovell@urv.cat

Authors

Luan Vittor Tavares Duarte de Alencar − *Department of Chemical Engineering, ETSEQ, Universitat Rovira i Virgili, 43007 Tarragona, Spain; Programa de Engenharia Química (PEQ/COPPE), Universidade Federal do Rio de Janeiro (UFRJ), 21941-909 Rio de Janeiro, RJ, Brazil*

Sabrina Belén Rodríguez-Reartes − *Department of Chemical Engineering, ETSEQ, Universitat Rovira i Virgili, 43007 Tarragona, Spain; Departamento de Ingeniería Química, Universidad Nacional del Sur (UNS), Bahía Blanca (8000), Argentina; Planta Piloto de Ingeniería Química—PLAPIQUI (UNS-CONICET), Bahía Blanca 8000, Argentina;* orcid.org/0000-0002-1430-2953

Frederico Wanderley Tavares − *Programa de Engenharia Química (PEQ/COPPE), Universidade Federal do Rio de Janeiro (UFRJ), 21941-909 Rio de Janeiro, RJ, Brazil; Engenharia de Processos Químicos e Bioquímicos, Escola de Química (EPQB), Universidade Federal do Rio de Janeiro (UFRJ), 21941-909 Rio de Janeiro, RJ, Brazil;* orcid.org/0000-0001-8108-1719

Complete contact information is available at: https://pubs.acs.org/10.1021/acssuschemeng.5c06167

Notes

The authors declare no competing financial interest.

■ ACKNOWLEDGMENTS

The authors are thankful to B. González Barramuño for his help on the numerical resolution of the Flash calculations of this manuscript. This work was done in the framework of projects NEW-F-Tech (ref: TED2021-130959B-I00) and REFCICLA (ref: PID2023-149713OB-I00) funded by MCIN/AEI/10.13039/501100011033/and by the European Union NextGenerationEU/PRTR. Additional funding from AGAUR as a Consolidated Research Group (SGR 2021-00738) and from the Chair on Energy Transition URV-Fundación Repsol are appreciated. L.V.T.D Alencar thanks the financial support from the Coordenação de Aperfeiçoamento de Pessoal de Nível Superior—Brasil (CAPES)—Finance Code 001; and Conselho Nacional de Desenvolvimento Científico e Tecnológico (CNPq—426956/2016-8). F.W. Tavares thanks ANP-Petrobras and FAPERJ for financial support. S. B. Rodriguez Reartes acknowledges the financial support of the "María Zambrano" grant (2021 URV-MZ-19) awarded by Universitat Rovira i Virgili (URV) for the requalification of the Spanish university system for 2021−2023.

■ REFERENCES

(1) Liao, X.; Chen, C.; Shi, P.; Yue, L. Determination of melamine in milk based on β-cyclodextrin modified carbon nanoparticles via host-guest recognition. *Food Chem.* **2021**, *338*, 127769.

(2) Zeng, S.; Dong, H.; Bai, Y.; Zhang, X.; Zhang, S. New technology of ionic liquid-based NH3/CO2 separation from melamine tail gas. *Green Chem. Eng.* **2020**, *1* (1), 5.

(3) Xue, X.; Zhang, Q.; Liu, Y.; Guo, Q.; Jiao, W.; Zhang, C. Selective absorption process intensification of ammonia from melamine exhaust gas using a counter airflow shear-rotating packed bed. *J. Environ. Chem. Eng.* **2022**, *10* (6), 108760.

(4) Ndegwa, P. M.; Hristov, A. N.; Arogo, J.; Sheffield, R. E. A review of ammonia emission mitigation techniques for concentrated animal feeding operations. *Biosyst. Eng.* **2008**, *100* (4), 453−469.

(5) Deng, D.; Deng, X.; Duan, X.; Gong, L. Protic guanidine isothiocyanate plus acetamide deep eutectic solvents with low viscosity for efficient NH3 capture and NH3/CO2 separation. *J. Mol. Liq.* **2021**, *324*, 114719.

(6) Xiang, X.; Guo, L.; Wu, X.; Ma, X.; Xia, Y. Urea formation from carbon dioxide and ammonia at atmospheric pressure. *Environ. Chem. Lett.* **2012**, *10* (3), 295−300.

(7) Zhuang, Q.; Clements, B.; Li, Y. From ammonium bicarbonate fertilizer production process to power plant CO2 capture. *Int. J. Greenh. Gas Control* **2012**, *10*, 56−63.

(8) Duan, Y.; Zhan, G.; Chang, F.; Shi, S.; Zeng, S.; Dong, H.; Abildskov, J.; Kjøbsted Huusom, J.; Zhang, X. Process simulation and evaluation for NH3/CO2 separation from melamine tail gas with protic ionic liquids. *Sep. Purif. Technol.* **2022**, *288*, 120680.
(9) Liu, X.; Chen, Y.; Zeng, S.; Zhang, X.; Liang, X.; Gani, R.; Kontogeorgis, G. M. Separation of NH3/CO2 from melamine tail gas with ionic liquid: Process evaluation and thermodynamic properties modelling. *Sep. Purif. Technol.* **2021**, *274*, 119007.
(10) Prabhune, A.; Dey, R. Green and sustainable solvents of the future: Deep eutectic solvents. *J. Mol. Liq.* **2023**, *379*, 121676.
(11) Smith, E. L.; Abbott, A. P.; Ryder, K. S. Deep Eutectic Solvents (DESs) and Their Applications. *Chem. Rev.* **2014**, *114* (21), 11060−11082.
(12) Zhang, Q.; De Oliveira Vigier, K.; Royer, S.; Jérôme, F. Deep eutectic solvents: syntheses, properties and applications. *Chem. Soc. Rev.* **2012**, *41* (21), 7108−7146.
(13) Pavlić, B.; Mrkonjić, Z.; Teslić, N.; Kljakić, A. C.; Pojić, M.; Mandić, A.; Stupar, A.; Santos, F.; Duarte, A. R. C.; Mišan, A. Natural Deep Eutectic Solvent (NADES) Extraction Improves Polyphenol Yield and Antioxidant Activity of Wild Thyme (Thymus serpyllum L.) Extracts. *Molecules* **2022**, *27* (5), 1508.
(14) Sarmad, S.; Mikkola, J.-P.; Ji, X. Carbon Dioxide Capture with Ionic Liquids and Deep Eutectic Solvents: A New Generation of Sorbents. *ChemSusChem* **2017**, *10* (2), 324−352.
(15) Zhang, Y.; Ji, X.; Lu, X. Choline-based deep eutectic solvents for CO2 separation: Review and thermodynamic analysis. *Renew. Sustain. Energy Rev.* **2018**, *97*, 436−455.
(16) Marcus, Y. Gas solubilities in deep eutectic solvents. *Monatsh. Chem.* **2018**, *149* (2), 211−217.
(17) Zhang, W.; Cheng, S.; Zhai, X.; Sun, J.; Hu, X.; Pei, H.; Chen, G. Green and Efficient Extraction of Polysaccharides From Poria cocos F.A. Wolf by Deep Eutectic Solvent. *Nat. Prod. Commun.* **2020**, *15* (2), 1934578X19900708.
(18) Xu, K.; Wang, Y.; Ding, X.; Huang, Y.; Li, N.; Wen, Q. Magnetic solid-phase extraction of protein with deep eutectic solvent immobilized magnetic graphene oxide nanoparticles. *Talanta* **2016**, *148*, 153−162.
(19) Li, N.; Wang, Y.; Xu, K.; Huang, Y.; Wen, Q.; Ding, X. Development of green betaine-based deep eutectic solvent aqueous two-phase system for the extraction of protein. *Talanta* **2016**, *152*, 23−32.
(20) Zhang, Y.; Zhu, C.; Fu, T.; Gao, X.; Ma, Y.; Li, H. Z. CO2 absorption and desorption performance by ChCl-MEA-PZ deep eutectic solvent aqueous solutions. *Sep. Purif. Technol.* **2024**, *330*, 125275.
(21) Oke, E. A. Sustainable advancements in hazardous gases capture: Harnessing the potential of deep eutectic solvents. *Sustain. Chem. Environ.* **2024**, *6*, 100083.
(22) Warrag, S. E. E.; Peters, C. J.; Kroon, M. C. Deep eutectic solvents for highly efficient separations in oil and gas industries. *Curr. Opin. Green Sustainable Chem.* **2017**, *5*, 55−60.
(23) García, G.; Aparicio, S.; Ullah, R.; Atilhan, M. Deep Eutectic Solvents: Physicochemical Properties and Gas Separation Applications. *Energy Fuels* **2015**, *29* (4), 2616−2644.
(24) Zhong, F.-Y.; Huang, K.; Peng, H.-L. Solubilities of ammonia in choline chloride plus urea at (298.2−353.2) K and (0−300) kPa. *J. Chem. Thermodyn.* **2019**, *129*, 5−11.
(25) Zhang, J.; Zheng, L.; Fang, S.; Zhang, H.; Cai, Z.; Huang, K.; Jiang, L. Efficient and reversible separation of NH3 by deep eutectic solvents with multiple active sites and low viscosities. *Chin. J. Chem. Eng.* **2024**, *67*, 97−105.
(26) Chen, Y.; Han, X.; Liu, Z.; Yu, D.; Guo, W.; Mu, T. Capture of Toxic Gases by Deep Eutectic Solvents. *ACS Sustainable Chem. Eng.* **2020**, *8* (14), 5410−5430.
(27) Shao, P.; Xiong, W.; Chen, P.; Liu, F.; Chen, T.; Zhao, T. Halogen-free deep eutectic solvents with multiple active sites for efficient absorption of ammonia. *Sep. Purif. Technol.* **2024**, *330*, 125390.
(28) Chapman, W. G.; Gubbins, K. E.; Jackson, G.; Radosz, M. SAFT: Equation-of-state solution model for associating fluids. *Fluid Phase Equilib.* **1989**, *52*, 31−38.
(29) Chapman, W. G.; Gubbins, K. E.; Jackson, G.; Radosz, M. New reference equation of state for associating liquids. *Ind. Eng. Chem. Res.* **1990**, *29* (8), 1709−1721.
(30) Gross, J.; Sadowski, G. Perturbed-Chain SAFT: An Equation of State Based on a Perturbation Theory for Chain Molecules. *Ind. Eng. Chem. Res.* **2001**, *40* (4), 1244−1260.
(31) Zubeir, L. F.; Held, C.; Sadowski, G.; Kroon, M. C. PC-SAFT Modeling of CO2 Solubilities in Deep Eutectic Solvents. *J. Phys. Chem. B* **2016**, *120* (9), 2300−2310.
(32) Yu, G.; Fu, Y.; Mu, W.; Wang, N.; Jovein, I. B.; Chen, B.; Sadowski, G.; Ji, X.; Held, C. CO2 capture with hydrophobic halogen-free natural deep eutectic solvents: Perturbed-Chain Statistical Associating Fluid Theory modeling and molecular insights. *AIChE J.* **2025**, *71* (8), No. e18878.
(33) Blas, F.; Vega, L. Thermodynamic behaviour of homonuclear and heteronuclear Lennard-Jones chains with association sites from simulation and theory. *Mol. Phys.* **1997**, *92* (1), 135−150.
(34) Alkhatib, I. I. I.; Ferreira, M. L.; Alba, C. G.; Bahamon, D.; Llovell, F.; Pereiro, A. B.; Araújo, J. M. M.; Abu-Zahra, M. R. M.; Vega, L. F. Screening of Ionic Liquids and Deep Eutectic Solvents for Physical CO2 Absorption by Soft-SAFT Using Key Performance Indicators. *J. Chem. Eng. Data* **2020**, *65* (12), 5844−5861.
(35) Lloret, J. O.; Vega, L. F.; Llovell, F. Accurate description of thermophysical properties of Tetraalkylammonium Chloride Deep Eutectic Solvents with the soft-SAFT equation of state. *Fluid Phase Equilib.* **2017**, *448*, 81−93.
(36) Ojeda, R. M.; Llovell, F. Soft-SAFT Transferable Molecular Models for the Description of Gas Solubility in Eutectic Ammonium Salt-Based Solvents. *J. Chem. Eng. Data* **2018**, *63* (7), 2599−2612.
(37) Jovell, D.; B Gómez, S.; Zakrzewska, M. E.; Nunes, A. V. M.; Araújo, J. M. M.; Pereiro, A. B.; Llovell, F. Insight on the Solubility of R134a in Fluorinated Ionic Liquids and Deep Eutectic Solvents. *J. Chem. Eng. Data* **2020**, *65* (10), 4956−4969.
(38) Demirbek, M. G.; Rodriguez Reartes, S. B.; Llovell, F. Thermodynamic Analysis of the Absorption of Common Refrigerants in Fluorinated Deep Eutectic Solvents. *Fluid Phase Equilib.* **2024**, *581*, 114077.
(39) Johnson, J. K.; Zollweg, J. A.; Gubbins, K. E. The Lennard-Jones equation of state revisited. *Mol. Phys.* **1993**, *78* (3), 591−618.
(40) Wertheim, M. S. Fluids with highly directional attractive forces. I. Statistical thermodynamics. *J. Stat. Phys.* **1984**, *35* (1), 19−34.
(41) Wertheim, M. S. Fluids with highly directional attractive forces. II. Thermodynamic perturbation theory and integral equations. *J. Stat. Phys.* **1984**, *35* (1), 35−47.
(42) Wertheim, M. S. Fluids with highly directional attractive forces. III. Multiple attraction sites. *J. Stat. Phys.* **1986**, *42* (3), 459−476.
(43) Wertheim, M. S. Fluids with highly directional attractive forces. IV. Equilibrium polymerization. *J. Stat. Phys.* **1986**, *42* (3), 477−492.
(44) Gubbins, K. E.; Twu, C. H. Thermodynamics of polyatomic fluid mixtures—I theory. *Chem. Eng. Sci.* **1978**, *33* (7), 863−878.
(45) Jog, P. K.; Sauer, S. G.; Blaesing, J.; Chapman, W. G. Application of Dipolar Chain Theory to the Phase Behavior of Polar Fluids and Mixtures. *Ind. Eng. Chem. Res.* **2001**, *40* (21), 4641−4648.
(46) Blas, F. J.; Vega, L. F. Prediction of Binary and Ternary Diagrams Using the Statistical Associating Fluid Theory (SAFT) Equation of State. *Ind. Eng. Chem. Res.* **1998**, *37* (2), 660−674.
(47) Alkhatib, I. I. I.; Pereira, L. M. C.; Torne, J.; Vega, L. F. Polar soft-SAFT: theory and comparison with molecular simulations and experimental data of pure polar fluids. *Phys. Chem. Chem. Phys.* **2020**, *22* (23), 13171−13191.
(48) Alencar, L. V. T. D.; Rodriguez-Reartes, S. B.; Tavares, F. W.; Llovell, F. A consistent framework to characterize the impact of co-solvents in the key process thermophysical properties of choline chloride-based DESs. *J. Ind. Eng. Chem.* **2024**, *132*, 279−290.

https://doi.org/10.1021/acssuschemeng.5c06167
ACS Sustainable Chem. Eng. 2025, 13, 15097−15106

(49) Pedrosa, N.; Pàmies, J. C.; Coutinho, J. A. P.; Marrucho, I. M.; Vega, L. F. Phase Equilibria of Ethylene Glycol Oligomers and Their Mixtures. *Ind. Eng. Chem. Res.* **2005**, *44* (17), 7027−7037.
(50) Crespo, E. A.; Silva, L. P.; Lloret, J. O.; Carvalho, P. J.; Vega, L. F.; Llovell, F.; Coutinho, J. A. P. A methodology to parameterize SAFT-type equations of state for solid precursors of deep eutectic solvents: the example of cholinium chloride. *Phys. Chem. Chem. Phys.* **2019**, *21* (27), 15046−15061.
(51) Dias, A. M. A.; Carrier, H.; Daridon, J. L.; Pàmies, J. C.; Vega, L. F.; Coutinho, J. A. P.; Marrucho, I. M. Vapor−Liquid Equilibrium of Carbon Dioxide−Perfluoroalkane Mixtures: Experimental Data and SAFT Modeling. *Ind. Eng. Chem. Res.* **2006**, *45* (7), 2341−2350.
(52) Llovell, F.; Marcos, R. M.; MacDowell, N.; Vega, L. F. Modeling the Absorption of Weak Electrolytes and Acid Gases with Ionic Liquids Using the Soft-SAFT Approach. *J. Phys. Chem. B* **2012**, *116* (26), 7709−7718.
(53) Gui, X.; Tang, Z.; Fei, W. Solubility of CO2 in Alcohols, Glycols, Ethers, and Ketones at High Pressures from (288.15 to 318.15) K. *J. Chem. Eng. Data* **2011**, *56* (5), 2420−2429.
(54) Leron, R. B.; Li, M.-H. Solubility of carbon dioxide in a choline chloride−ethylene glycol based deep eutectic solvent. *Thermochim. Acta* **2013**, *551*, 14−19.
(55) Li, X.; Hou, M.; Han, B.; Wang, X.; Zou, L. Solubility of CO2 in a Choline Chloride + Urea Eutectic Mixture. *J. Chem. Eng. Data* **2008**, *53* (2), 548−550.
(56) Leron, R. B.; Li, M.-H. Solubility of carbon dioxide in a eutectic mixture of choline chloride and glycerol at moderate pressures. *J. Chem. Thermodyn.* **2013**, *57*, 131−136.
(57) Zhou, H.; Zhang, S.; Gao, F.; Bai, X.; Sha, Z. Solubility of Ammonia in Ethylene Glycol Between 303 and 323 K under Low Pressure from 0.030 to 0.101 MPa. *Chin. J. Chem. Eng.* **2014**, *22* (2), 181−186.
(58) Malik, A.; Kashyap, H. K. Solvation Shell Structures of Ammonia in Reline and Ethaline Deep Eutectic Solvents. *J. Phys. Chem. B* **2023**, *127* (11), 2499−2510.
(59) Duan, X.; Gao, B.; Zhang, C.; Deng, D. Solubility and thermodynamic properties of NH3 in choline chloride-based deep eutectic solvents. *J. Chem. Thermodyn.* **2019**, *133*, 79−84.
(60) Cadena, C.; Anthony, J. L.; Shah, J. K.; Morrow, T. I.; Brennecke, J. F.; Maginn, E. J. Why Is CO2 So Soluble in Imidazolium-Based Ionic Liquids? *J. Am. Chem. Soc.* **2004**, *126* (16), 5300−5308.
(61) Llovell, F.; Oliveira, M. B.; Coutinho, J. A. P.; Vega, L. F. Solubility of greenhouse and acid gases on the [C4mim][MeSO4] ionic liquid for gas separation and CO2 conversion. *Catal. Today* **2015**, *255*, 87−96.
(62) Sander, R.; Acree, W. E.; Visscher, A. D.; Schwartz, S. E.; Wallington, T. J. Henry's law constants (IUPAC Recommendations 2021). *Pure Appl. Chem.* **2022**, *94* (1), 71−85.
(63) Shahbaz, K.; Baroutian, S.; Mjalli, F. S.; Hashim, M. A.; AlNashef, I. M. Densities of ammonium and phosphonium based deep eutectic solvents: Prediction using artificial intelligence and group contribution techniques. *Thermochim. Acta* **2012**, *527*, 59−66.
(64) Hayler, H. J.; Perkin, S. The eutectic point in choline chloride and ethylene glycol mixtures. *Chem. Commun.* **2022**, *58* (91), 12728−12731.
(65) Huang, J.-Y.; Jiang, W.-J.; Xiao, P.; Fan, Z.-T.; Zhong, F.-Y.; Peng, H.-L.; Du, J.; Huang, K. Physical Properties and NH3 Solubilities of Deep Eutectic Solvents Formed by Choline Chloride and Glycols. *Fluid Phase Equilib.* **2021**, *529*, 112871.
(66) Mejía, A.; Müller, E. A.; Chaparro Maldonado, G. SGTPy: A Python Code for Calculating the Interfacial Properties of Fluids Based on the Square Gradient Theory Using the SAFT-VR Mie Equation of State. *J. Chem. Inf. Model.* **2021**, *61* (3), 1244−1250.
(67) Chaparro, G.; Mejía, A. Phasepy: A Python based framework for fluid phase equilibria and interfacial properties computation. *J. Comput. Chem.* **2020**, *41* (29), 2504−2526.

https://doi.org/10.1021/acssuschemeng.5c06167
ACS Sustainable Chem. Eng. 2025, 13, 15097−15106